Available online at www.sciencedirect.com
SCIENCE DIRECT®
Journal of Nuclear Materials 337–339 (2005) 50–54
journal of nuclear materials
www.elsevier.com/locate/jnucmat

ITER divertor performance in conditions of carbon re-erosion ☆

A.S. Kukushkin [a,*], H.D. Pacher [b], D.P. Coster [c], G.W. Pacher [d], D. Reiter [e]

[a] *ITER Joint Central Team, Garching Joint Work Site, Garching D-85748, Germany*
[b] *INRS-Energie, Matériaux, et Télécommunciations, Varennes, Québec J3X 1S2, Canada*
[c] *Max-Planck Institut für Plasmaphysik, Garching D-85748, Germany*
[d] *Hydro-Québec, Varennes, Québec J3X 1S1, Canada*
[e] *FZ Jülich, Jülich D-52425, Germany*

Abstract

The effect of carbon re-erosion in a mixed-material environment on the results of ITER edge plasma modelling is presented. Divertor performance is investigated with varying erosion rate of re-deposited carbon and varying connection length. The results are unified as scaling relations in the edge parameters, allowing meaningful comparison as model parameters are varied and providing effective boundary conditions for core plasma modelling.

PACS: 52.25.Vy; 52.40.Hf; 52.65.Kj; 52.65.Pp
Keywords: B2/Eirene; Erosion and deposition; Edge modelling; ITER

1. Introduction

Originally, the boundary conditions for the plasma-facing materials in ITER modelling [1–4] assumed that carbon sputtered from the targets was completely absorbed at the first wall (Be), baffle (W) and dome (W), ensuring low edge carbon concentration. However, the deposited carbon can be re-eroded. Where the D/T fluxes are high enough, this deposited carbon will be completely removed (induced carbon recycling), and the resulting surface will be metallic and will absorb no carbon. Where the fluxes are low, the deposited carbon flux exceeds the eroded flux and carbon accumulates. Since the surface properties depend on the particle fluxes, the boundary conditions (net erosion or deposition) representing realistic surfaces (RS) must be

☆ This report was prepared as an account of work undertaken within the framework of ITER Transitional Arrangements (ITA). These are conducted by the Participants: China, the European Atomic Energy Community, Japan, Korea, the Russian Federation, and the United States of America, under the auspices of the International Atomic Energy Agency. The views and opinions expressed herein do not necessarily reflect those of the Participants to the ITA, the IAEA or any agency thereof. Dissemination of the information in this paper is governed by the applicable terms of the former ITER EDA Agreement.

* Corresponding author. Address: ITER IT, Max-Plank Institut für Plasmaphysik, Boltzmannstr. 2, Garching D-85748, Germany. Tel.: +49 89 3299 4122; fax: +49 89 3299 4165.
E-mail address: kukusha@itereu.de (A.S. Kukushkin).

0022-3115/$ - see front matter
doi:10.1016/j.jnucmat.2004.10.006

determined iteratively to be consistent with the solution, as discussed below. Initial modelling studies [5] showed that the parameters of the edge plasma are strongly affected because the carbon ion residence time increases, and $Z_{\rm eff}$ values of ~1.7 at the separatrix were obtained. In the present investigation, the sputter yield for deposited carbon is varied to adjust to experimental observations [6] (see below), and edge plasma performance is analysed for steady-state ITER operation (lower plasma current, hence higher safety factor q_{95} [7]) with the same RS model.

2. Model features

We use the B2-Eirene code package, version solps4.0 [8], combining a full multi-fluid description of the electrons and D, He, and C ions (B2), and a Monte-Carlo neutral description in toroidal geometry (Eirene), with the parameters and geometry as in [3–5]. The parallel plasma transport is flux-limited, and no drifts in the SOL plasma are considered. The radial transport is described by constant particle and heat diffusivities, $D_\perp = 0.3$ m^2/s and $\chi_\perp = 1$ m^2/s, no pinch. The computational grid is limited by the second separatrix, not by the wall, and decay lengths of 3 cm for all plasma densities and temperatures are set as boundary conditions there. These boundary conditions imply an outward convection with $v_\perp = 10$ m/s for all ion species which contributes a constant 43% of the energy outflow at the grid edge. At the core-edge interface, we specify the total incident power in electrons and ions, the DT ion flux, zero C ion flux, and zero He^+ density; the He^{2+} density is adjusted to yield the fusion-produced flux with the given pumping speed. 100% recycling of DT and He is assumed at every material surface, and the pumping speed is set by specifying an albedo for neutrals at the pump duct. The DT and C ion densities result from the balance between the input and output fluxes, a procedure that ensures stability of the particle balance in density scans ranging from partially attached to fully detached divertor plasmas.

The recycling behaviour of C particles depends on the surface type. At the targets, carbon is eroded by physical and chemical sputtering by all relevant ions and atoms, and impinging C particles stick there, as is also the case for a wall made of carbon. For the RS model, the boundary conditions are iterated. On each iteration, a long B2-Eirene run (~10 ms, until convergence) precedes an Eirene stand-alone diagnostic run, which determines at every point whether erosion or deposition dominates if the surface there were carbon. Subsequently, the appropriate local boundary conditions are assigned. The process continues until the surface properties remain unchanged, typically requiring three to eight iterations.

3. Effect of carbon re-erosion

For a typical ITER case with chemical erosion yield $Y_{\rm ch} = 0.01$ for both the original and deposited carbon, and with fuelling primarily by gas puffing, the lower part of the outboard first wall is deposition-dominated [5]. This area increases when core fuelling is applied, since then D–T recycling in the main chamber is lower. However, JET experimental results [6] indicate that the first wall in the main chamber is mostly a net erosion area. This could be explained if the effective $Y_{\rm ch}$ for the deposits, in areas of low fluxes, were larger than for solid carbon targets. This would occur if $Y_{\rm ch}$ has a strong flux dependence [9] or could be a consequence of a different structure of the deposits and of solid carbon [10]. We therefore undertook a survey using constant $Y_{\rm ch} = 0.01$ for the targets and multiplying it by a factor $Y_{\rm C\_dep} = 1$, 2, 4, and 8 for the deposits. The results (Fig. 1(a)) show the expected trend: net deposition becomes significantly lower at $Y_{\rm C\_dep} = 4$, and disappears at $Y_{\rm C\_dep} = 8$. Therefore an increase of $Y_{\rm ch}$ for the deposits by an order of magnitude would result in a carbon-free first wall in ITER, at least for relatively strong gas puffing.

As in the preceding studies with carbon-absorbing metal walls [3,4] and initial studies with carbon walls and the RS model [5], the present, more comprehensive study with variation of $Y_{\rm C\_dep}$ exhibits a two-regime behaviour in density scans, i.e. a transition from a regime 'a' for which the separatrix DT density $n_{\rm DT\_sep}$ increases with the gas pressure in the private flux region (PFR), $p_{\rm DT} = \Gamma_{\rm DT}/S_{\rm DT}$, to a regime 'b' where it saturates ($\Gamma_{\rm DT}$ is the total DT throughput and $S_{\rm DT}$ the pumping

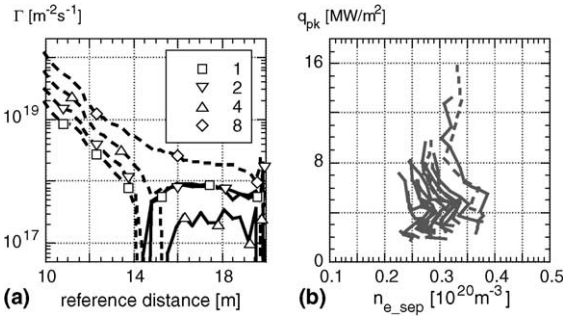

Fig. 1. (a) Profiles of net C deposition (solid lines) and virtual net C erosion (dashed) on the outer first wall of ITER for different $Y_{\rm C\_dep}$. Distance 10 m is the top, 20 m is the bottom of the first wall at the top of the outboard target. No net C deposition is seen for $Y_{\rm C\_dep} = 8$. (b) Peak power at the divertor plate $q_{\rm pk}$ vs. average separatrix electron density. Different curves correspond to density scans at $P_{\rm SOL} = 86$, 100, and 130 MW, for RS model with $Y_{\rm C\_dep} = 1$, 2, 4, and 8, and for full carbon wall in inductive operation (dotted lines), and at $P_{\rm SOL} = 80$, 100, and 120 MW for RS model with $Y_{\rm C\_dep} = 1$ in steady state.

speed). The obtained edge parameters are widely dispersed, Fig. 1(b). From the examination of density scans for various SOL power, fuelling conditions, wall conditions, safety factor, and pumping speed, the transition point (TP) between regimes 'a' and 'b' can be expressed in terms of an appropriately normalised neutral pressure in the PFR as $\mu = 1$,

$$\mu \equiv p_{\mathrm{DT}\#} P_{\mathrm{SOL}\#}^{-0.87} f_{\mathrm{f}}^{-0.8} f_{\mathrm{w}}^{-1} q_{95\#}^{-0.27}, \quad (1)$$

(the subscript # denotes here and below the normalised quantities; normalisations given in Table 1). μ involves the total power input to the SOL P_{SOL} and a 'fuelling factor' $f_{\mathrm{f}} \equiv 1 + 0.18\Gamma_{\mathrm{core}}/\Gamma_{\mathrm{DT}}$, where Γ_{core} is the core fuelling rate [4]. (The present scaling with f_{f} differs somewhat from that of [4] for carbon-absorbing walls.) The variation of the TP as $Y_{\mathrm{C\_dep}}$ is set to 1, 2, 4, and 8, for the RS can be expressed by introducing a 'wall factor' f_{w} of 1, 0.83, 0.71, and 0.71, respectively, and of 0.84 for full carbon walls. Therefore, the pressure at which the plasma detaches from the inner divertor decreases as the re-erosion of the deposited carbon increases, and this effect saturates. Steady state cases ($q_{95} = 4.5$ [7]) are accommodated by introducing $q_{95\#}$ in Eq. (1).

Use of the normalised pressure leads to universal curves in the form of power law scalings in parameter space. Fig. 2(a) shows the DT density at the separatrix in terms of μ and demonstrates saturation at $\mu = 1$. Fig. 2(b) shows that this is related to complete detachment of the plasma at the inner divertor plate (the maximum temperature there drops below 2 eV) which occurs at $\mu = 1.17$. To avoid possible confinement degradation by excessive neutral influx around the X point to the core, ITER operation is conservatively restricted to regime 'a' ($\mu < 1$), where the density does not yet saturate and the inner divertor is not yet completely detached.

$n_{\mathrm{DT\_sep}}$ (Fig. 2(a)) and q_{pk} (Fig. 3(a)) for all these cases are well fitted by universal scaling relations. The helium separatrix density $n_{\mathrm{He\_sep}}$ (Fig. 3(b)) and He atom influx to the core $\Gamma_{\mathrm{He\_n\_sep}}$ can be described by a three-part scaling with μ (Table 1): a variation as μ^{-2}

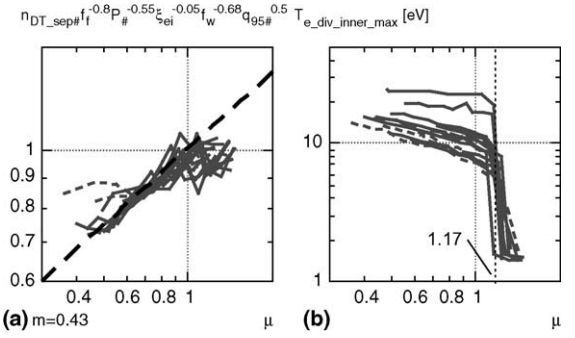

Fig. 2. (a) Normalised DT density at the separatrix and (b) maximum temperature at the inner divertor versus normalised PFR neutral pressure μ for the data sets from Fig. 1(b). Normalisations here and in Figs. 3 and 4 are from Table 1. Dashed line indicates the fit, 'm' its slope.

Table 1
Coefficients in regime 'a' scaling for RS and full carbon walls (e.g., $q_{\mathrm{pk}} = 3.8(p_{\mathrm{DT}}/(8.5\ \mathrm{Pa}))^{-1.17} f_{\mathrm{f}}^{0.34} (P_{\mathrm{SOL}}/(100\ \mathrm{MW}))^{2.28} f_{\mathrm{w}}^{0.8} (q_{95}/3)^{-0.18}$ [MW/m^2])

Regime a		p_{DT} [p]	f_{He}	f_{f}	S_{DT} [S]	P_{SOL} [P]	ξ_{ei}	f_{w}	q_{95}
	Scale	8.5	1	1	20	100	1	1	3
q_{pk} [q]	3.8	−1.17	0	0.34	0	2.28	0	0.8	−0.18
$n_{\mathrm{DT\_sep}}$ [n]	0.3	0.43	0	0.46	0	0.18	0.05	0.25	−0.62
$\Gamma_{\mathrm{DT\_n\_sep}}$ [Γ]	15	0.36	0	−4.59	0.3	−0.31	0	0.08	−0.3
$T_{\mathrm{e\_sep}}$ [eV]	170	−0.12	0	−0.1	−0.02	0.42	0.05	−0.04	0.53
$T_{\mathrm{i\_sep}}$ [eV]	300	−0.24	0	−0.41	−0.04	0.57	−0.12	−0.06	0.56
$n_{\mathrm{C\_sep}}$ [n]	0.0056 (0.0067)	0	0	0	0	0.54	−0.13	−0.77	−0.32
$\Gamma_{\mathrm{C\_targ}}$ [Γ]	230 (360)	0.58	0	−0.46	0	0.25	0	2.82	−0.74
$P_{\mathrm{imp\_rad}}$ [P]	55	0.14	0	−0.11	0	1.23	0	−0.43	0.24
$n_{\mathrm{He\_sep}}$ [n]									
$\mu > 0.85$	0.0027	−2	1	−2.4	−1	1.74	−0.1	2	−0.31
$0.6 < \mu < 0.85$	0.0038	0	1	−4	−1	0	−0.1	0	−0.85
$\mu < 0.6$	0.00135	−2	1	−2.4	−1	1.74	−0.1	2	−0.31
$\Gamma_{\mathrm{He\_n\_sep}}$ [Γ]									
$\mu > 0.85$	0.26	−2	1	−0.4	−1	1.74	0	2	0.54
$0.6 < \mu < 0.85$	0.36	0	1	−2	−1	0	0	0	0
$\mu < 0.6$	0.13	−2	1	−0.4	−1	1.74	0	2	0.54

Values in brackets are for full carbon walls if different from RS.
[Γ] = [Pa m^3/s], [n] = [10^{20} m^{-3}], [T] = [eV], [p] = [Pa], [P] = [MW], [q] = [MW/m^2], [S] = [m^3/s]. For electron density use $n_{\mathrm{e\_sep}} = n_{\mathrm{DT\_sep}} + 2n_{\mathrm{He\_sep}} + 5.6n_{\mathrm{C\_sep}}$. ξ_{ei} is the ratio of electron to ion power to the SOL. $f_{\mathrm{He}} = 0.21(5Q/(Q+5))(1 - f_{\mathrm{rad}})^{-1}$ [4]. Three-part helium scaling depends on values of μ (see the text).

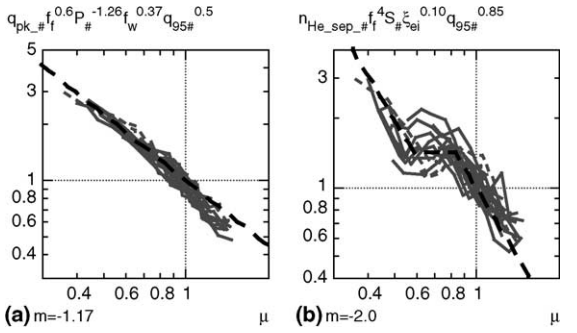

Fig. 3. (a) Normalised peak power per unit area at the divertor plate and (b) normalised He density at the separatrix vs. μ for the data sets of Fig. 1(b).

for $\mu > 0.85$, a 'plateau' as μ^0 for $0.6 < \mu < 0.85$, and a variation as $0.5\mu^{-2}$ for $\mu < 0.6$. Use of the scaling for $\mu > 0.85$ is therefore conservative. The results confirm that, for the reference case (RS, $Y_{C\_dep} = 1$, $q_{95} = 3$, $P_{SOL} = 100$ MW) at the highest divertor pressure ($\mu = 1$), helium pumping is relatively uncritical, i.e. the He concentration at the separatrix is below 1% and $\Gamma_{He\_n\_sep} < 1/3$ of the helium production rate of 0.64 Pa m^3/s resulting from fusion reactions.

For the carbon wall and RS cases (in contrast to the metal wall cases [3,4]) the carbon density remains nearly constant as the divertor pressure varies, and the carbon flux is also close to a unique scaling. However, Fig. 4 shows that at the same μ full carbon walls have 20% higher carbon density at the separatrix n_{C_sep} and 60% higher net carbon erosion flux Γ_{C_targ} than the RS cases, reflecting the carbon release in the erosion-dominated areas for that case. Since more of the wall becomes a net erosion area as Y_{C_dep} increases, and consequently more carbon is returned to the plate and less is deposited elsewhere, Γ_{C_targ} decreases.

Fig. 5 shows variations of the plasma parameters at the TP ($\mu = 1$) as a function of Y_{C_dep}. Except for the

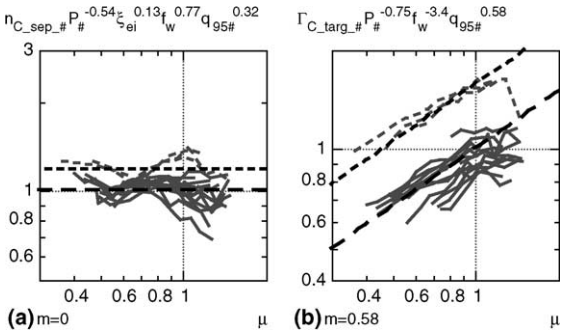

Fig. 4. (a) Normalised carbon density at the separatrix and (b) normalised carbon target erosion flux vs. μ for the data sets of Fig. 1(b). Carbon wall cases and scalings are shown dotted.

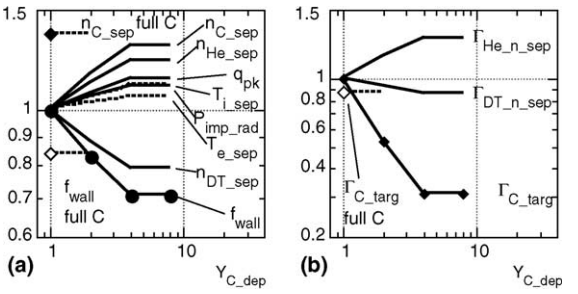

Fig. 5. Edge plasma parameters at the TP ($\mu = 1$) normalized to the reference case vs. Y_{C_dep} for RS and full carbon walls (marked 'full C').

carbon density and flux, the full carbon wall behaves as if it were a RS with $Y_{C\_dep} = 1.9$. As Y_{C_dep} increases, n_{DT_sep} and Γ_{C_targ} at $\mu = 1$ decrease but n_{C_sep}, n_{He_sep} and hence fuel dilution increase, as does q_{pk}.

The q_{95} dependence of the scalings (Table 1) shows that, in comparison to the reference inductive cases, the steady state cases at the same μ have around 20% lower separatrix densities (DT: 22%, C: 23%, He: 12%), 25% higher separatrix temperatures T_{i,e_sep}, 28% higher $\Gamma_{He\_n\_sep}$, 10% lower q_{pk}, 27% lower Γ_{C_targ} and 13% higher impurity radiation P_{imp_rad}.

4. Conclusions

We have developed a new methodology to model plasma-facing metal surfaces with realistic erosion-deposition of carbon eroded from the targets, namely, iterative adjustment of the material properties of the walls until they are consistent with the solution. Application of this technique to ITER shows that the re-erosion of deposits increases the residence time of carbon in the edge plasma, leading to higher C concentrations ($Z_{eff} \sim 1.7$ at the separatrix) and lower net erosion of C from the target. The C deposition outside the targets is therefore reduced, but quantitative assessment of corresponding co-deposition of tritium requires a further refinement of the model, including the chemistry and transport of hydrocarbons. An increase of the chemical sputtering yield for the deposited carbon reduces the deposition in the main chamber and the net erosion, rendering the deposition pattern closer to experimental observations on present-day machines.

New scalings have been developed for the edge plasma parameters, unifying the data obtained with different carbon re-erosion properties and different connection lengths. These scalings form a new set of boundary conditions for the core models, allowing analysis of the operational space of ITER in a consistent way [11,12], for both the standard inductive and steady-state operation.

References

[1] A.S. Kukushkin, G. Janeschitz, A. Loarte, H.D. Pacher, et al., J. Nucl. Mater. 290–293 (2001) 887.
[2] A.S. Kukushkin, H.D. Pacher, Plasma Phys. Contr. Fusion 44 (2002) 931.
[3] H.D. Pacher, A.S. Kukushkin, G.W. Pacher, et al., J. Nucl. Mater. 313–316 (2003) 657.
[4] A.S. Kukushkin, H.D. Pacher, G.W. Pacher, et al., Nucl. Fusion 43 (2003) 716.
[5] A.S. Kukushkin, H.D. Pacher, D. Coster, et al., in: Proc. 30th EPS Conference on Contr. Fusion and Plasma Phys., St. Petersburg, 2003, paper P-3.195.
[6] J. Likonen, S. Lehto, J.P. Coad, et al., Fusion Eng. Des. 66–68 (2003) 219.
[7] M. Shimada, A.E. Costley, G. Federici, et al., these Proceedings.
[8] D.P. Coster, X. Bonnin, B. Braams, et al., in: Proc. 19th IAEA Fusion Energy Conf., Lyon, 2002, paper TH/P2-13.
[9] J. Roth, A. Kirschner, R. Preuss, et al., these Proceedings.
[10] M.F. Stamp, S.K. Erents, W. Fundamenski, et al., J. Nucl. Mater. 290–293 (2001) 321.
[11] G.W. Pacher, H.D. Pacher, A.S. Kukushkin, et al., Nucl. Fusion 43 (2003) 188.
[12] G.W. Pacher, H.D. Pacher, G. Janeschitz, et al., Plasma Phys. Control. Fusion 46 (2004) A257.